INTERNATIONAL JOURNAL OF RESEARCH
In Advanced Engineering Technologies

Volume 6, Issue 3 MAY 2018

MODELING AND SIMULATION OF DC GRID BASED WIND POWER GENERATION IN A MICROGRID APPLICATION

[1]SHAIK MAHABOOB PEERA , [2]RAMI REDDY

[1]Mtech,(Student) Nalanda Institute Of Engineering And Technology
[2]Asst. professor, Nalanda Institute Of Engineering And Technology

ABSTRACT-In this paper we are implementing the dc grid based wind power generation system in a poultry farm. The proposed paper will allow the flexible operation of multiple parallel connected wind generators by eliminating the unbalances in the grid for providing the normal voltage and frequency synchronization. The model predictive control algorithm that will gives the better transient response regarding to the changes in the operating conditions is proposed for the control of the inverters. The performance of proposed dc grid wind power will analyze in MATLAB software.

INTRODUCTION

A dc microgrid based wind farm architecture in which each wind energy conversion unit consisting of a matrix converter, a high frequency transformer and a single-phase ac/dc converter is proposed. However, the proposed architecture increases the system complexity as three stages of conversion are required. In an investigation on the usefulness of the MPC in the control of parallel-connected inverters is conducted. In conventional practices, the control signals are clipped to stay within the constraints, thus the system will operate at the suboptimal point.

Poultry farming is the raising of domesticated birds such as chickens and ducks for the purpose of farming meat or eggs for food. Besides cooling the farms, the wind energy produced by the cooling fans can be harnessed using wind turbines (WTs) to reduce the farms' demand on the grid. The variability of wind speed in wind farms directly depends on the environmental and weather conditions while the wind speed in poultry farms is generally stable as it is generated by constant -speed ventilation fans.

Thus, the generation intermittency issues that affect the reliability of electricity supply and power balance are not prevalent in poultry farm wind energy systems. A dc micro grid based wind farm architecture in which the WTs are clustered into groups of four with each group connected to a converter is proposed. However, with the proposed architecture, the failure of one converter will result in all four WTs of the same group to be out of service. The DERs in dc micro grids are strongly coupled to each other and there must be a minimum level of coordination between the DERs and the controllers.. To regulate the output voltage and the power flow of the inverters commonly adopted control scheme contains an inner voltage and current loop and an external power loop.

These areas include improving the robustness of the controllers to topological and parametric uncertainties, and improving the transient response of the controllers. As the microgrid is required to operate stably in different operating conditions, the deployment of MPC for the control of the inverters offers better transient response with respect to the changes in the operating conditions and ensures a more robust microgrid operation. There are some research works on the implementation of MPC for the control of inverters.

An alternative solution using a dc grid based distribution network where the ac outputs of the wind generators (WGs) in a poultry farm are rectified to a common voltage at the dc grid is proposed in this paper. The most significant advantage of the proposed system is that only the voltage at the dc grid has to be controlled for parallel operation of several WGs without the need to synchronize the voltage, frequency and phase, thus allowing the WGs to be turned ON or OFF anytime without causing any disruptions.

To increase the controller's robustness against variations in the operating conditions when the microgrid operates in the grid-connected or islanded mode of operation as well as its capability to handle constraints, a model-based model predictive control (MPC) design is proposed in this paper for controlling the inverters. As the microgrid is required to operate stably in different operating conditions, the deployment of MPC for the control of the inverters offers better transient response with respect to the changes in the operating conditions and ensures a more robust microgrid operation. There are some research works on the implementation of MPC for the control of inverters.

In what follows, a comprehensive solution for the operation of a dc grid based wind power generation system in a microgrid is proposed for a poultry farm and the effectiveness of the proposed system is verified by simulation studies under different operating conditions.

SYSTEM DESCRIPTION AND MODELING

System Description

The overall configuration of the proposed dc grid based wind power generation system for the poultry farm is shown in Fig. 1. The system can operate either connected to or islanded from the distribution grid and consists of four 10 kW permanent magnet synchronous generators (PMSGs) which are driven by the variable speed WTs. The three-phase output of each PMSG is connected to a three-phase converter (i.e., converters A, B, C and D), which operates as a rectifier to regulate the dc output voltage of each PMSG to the desired level at the dc grid.

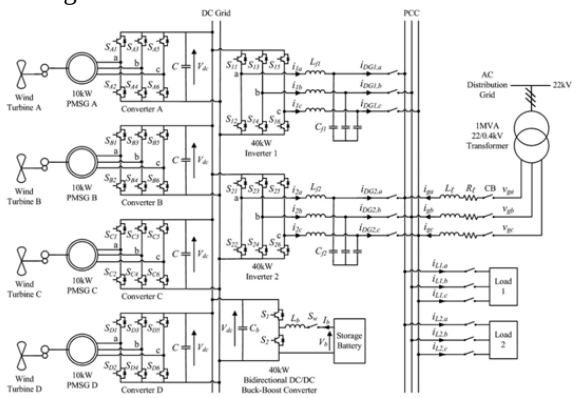

Fig. 1. Overall configuration of the proposed dc grid based wind power generation system in a micro grid.

This architecture minimizes the need to synchronize the frequency, voltage and phase, reduces the need for multiple inverters at the generation side, and provides the flexibility for the plug and play connection of WGs to the dc grid. The availability of the dc grid will also enable the supply of power to dc loads more efficiently by reducing another ac/dc conversion. The coordination of the converters and inverters is achieved through a centralized energy management system (EMS). The EMS controls and monitors the power dispatch by each WG and the load power consumption in the microgrid through a centralized server. To prevent excessive circulating currents between the inverters, the inverter output voltages of inverters 1 and 2 are regulated to the same voltage. Through the EMS, the output voltages of inverters 1 and 2 are continuously monitored to ensure that the inverters maintain the same output voltages.

During normal operation, the two inverters will share the maximum output from the PMSGs (i.e., each inverter shares 20 kW). The maximum power generated by each WT is estimated from the optimal wind power Pwt,opt as follows [23]:

$$P_{wt,opt} = k_{opt}\left(w_{r,opt}\right)^3 \quad (1)$$

$$k_{opt} = 0.5 C_{p,opt} \rho A \left(\frac{R}{\lambda_{opt}}\right)^3 \quad (2)$$

$$w_{opt} = \left(\frac{\lambda_{opt}}{R}\right) \quad (3)$$

where k opt is the optimized constant, ωr,opt is the WT speed for optimum power generation, Cp, opt is the optimum power coefficient of the turbine, ρ is the air density, A is the area swept by the rotor blades, λopt is the optimum tip speed ratio, v is the wind speed and R is the radius of the blade. When one inverter fails to operate or is under maintenance, the other inverter can handle the maximum power output of 40 kW from the PMSGs. The energy constraints of the SB in the proposed dc grid are determined based on the system-on-a-chip (SOC) limits given by

$$SOC_{min} < SOC \leq SOC_{max} \quad (4)$$

System Operation

When the microgrid is operating connected to the distribution grid, the WTs in the microgrid are responsible for providing local power support to the loads, thus reducing the burden of power delivered from the grid. The SB can be controlled to achieve different demand side management functions such as peak shaving and valley filling depending on the time-of-use of electricity and SOC of the SB. During islanded operation where the CBs disconnect the microgrid from the distribution grid, the WTs and the SB are only available sources to supply the load demand. The SB can supply for the deficit in real power to maintain the power balance of the microgrid as follows:

$$P_{wt} + P_{sb} = P_{loss} + P_l \quad (5)$$

Where Pwt is the real power generated by the WTs, Psb is the real power supplied by SB which is subjected to the constraint of the SB maximum power Psb, max that can be delivered during discharging and is given by

$$P_{sb} \leq P_{sb,max} \quad (6)$$

Ploss is the system loss, and Pl is the real power that is supplied to the loads.

AC/DC Converter Modeling

Fig. 2 shows the power circuit consisting of a PMSG which is connected to an ac/dc voltage source converter. The PMSG is modeled as a balanced three-phase ac voltage source esa, esb,esc with series resistance R s and inductance Ls. As shown in, the state equations for the PMSG currents isa, isb, isc and the dc output voltage Vdc of the converter can be expressed as follows:

$$L_s \frac{di_s}{dt} = -R_s L_s + e_s - KSV_{dc} \quad (7)$$

$$C = \frac{dV_{dc}}{dt} = i_s{}^T S - I_{dc} \quad (8)$$

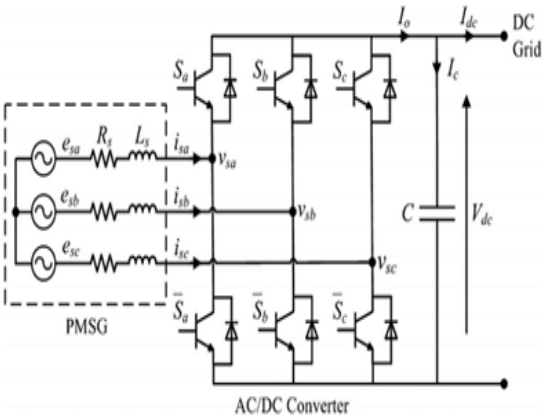

Fig. 2. Power circuit of a PMSG connected to an ac/dc voltage source converter.

Where

$$i_s = [i_{sa} \quad i_{sb} \quad i_{sc}]^T,\ e_s = [e_{sa} \quad e_{sb} \quad e_{sc}]^T$$

$$K = \begin{bmatrix} 2/3 & -1/3 & -1/3 \\ -1/3 & 2/3 & -1/3 \\ -1/3 & -1/3 & 2/3 \end{bmatrix}$$

$S = [S_a \quad S_b \quad S_c]^T$ is the ac/dc converter switching functions which are defined as

$$S_j = \begin{cases} 1, & S_j \ is\ ON \\ 0 & S_j \ is\ OFF \end{cases} \quad \text{for j= a,b,c} \qquad (9)$$

DC/AC Inverter Modeling

The two 40 kW three-phase dc/ac inverters which connect the dc grid to the point of common coupling (PCC) are identical, and the single-phase representation of the three-phase dc/ac inverter is shown in Fig. 3. To derive a state-space model for the inverter, Kirchhoff's voltage and current laws are applied to loop i and point x respectively, and the following equations are obtained:

$$L_f \frac{di}{dt} + iR + v_{dc} = uV_{dc} \qquad (10)$$

$$i_{DG} = i - i_{Cf} \qquad (11)$$

where Vdc is the dc grid voltage, u is the control signal, R is the inverter loss, Lf and Cf are the inductance and capacitance of the low-pass (LPF) filter respectively, iDG is the inverter output current, i is the current flowing through Lf , iCf is the current flowing through Cf , and vDG is the inverter output voltage.

Thus, the discrete state-space equations for the inverter model operating in the CCM can be expressed with sampling time Ts as follows:

$$x_g(k+1) = A_g x_g(k) + B_{g1} v_g(k) + B_{g2} u_g(k) \qquad (12)$$

$$y_g(k) = C_g x_g(k) + D_g v_g(k) \qquad (13)$$

where the subscript g represents the inverter model during grid connected operation, k is the discretized present time step, and

$$A_g = 1 - \frac{R}{L_f} T_S,\ \ B_{g1} = \begin{bmatrix} 0 & -\frac{T_S}{L_f} \end{bmatrix},$$

$$B_{g2} = \frac{v_{dc}}{L_f},\ C_g = 1,\ D_g = \begin{bmatrix} \frac{C_f}{T_S} & -\frac{C_f}{T_S} \end{bmatrix}$$

x g(k) = i(k) is the state vector; vg(k) = [vDG(k + 1) vDG(k)]T is the exogenous input; ug(k) is the control signal with −1 ≤ ug(k) ≤ 1; and yg(k) = iDG(k) is the output. The exogenous input vg(k) can be calculated using state estimation.

The voltage of the PCC will be maintained by the inverters when the microgrid is islanded from the grid. As compared to Ts, the rate of change of the inverter output current is much slower. Therefore, the following assumption is made when deriving the state-space equations for the inverter operating in the VCM:

$$\frac{di_{DG}}{dt} = 0 \qquad (14)$$

Based on the above mentioned assumption, the discrete statespace equations of the inverter model operating in the VCM can be expressed as follows

$$x_i(k+1) = A_i x_i(k) + B_i u_i(k) \qquad (15)$$

$$y_i(k) = C_i x_i(k) \qquad (16)$$

where the subscript i represents the model of the inverter during islanded operation and

xi(k) = [i(k) vDG(k) iDG(k)]^T is the state vector; ui(k) is the control signal with −1 ≤ ui(k) ≤ 1; and yi(k) = vDG(k) is the output. During islanded operation, the inverters are required to deliver all the available power from the PMSGs to the loads. Therefore, only the inverter output voltage is controlled and the output current is determined from the amount of available power.

CONTROL DESIGN

Control Design for the AC/DC Converter

Fig. 4 shows the configuration of the proposed controller for each ac/dc voltage source converter which is employed to maintain the dc output voltage Vdc of each converter and compensate for any variation in Vdc due to any power imbalance in the dc grid. The power imbalance will induce a voltage error (Vdc ∗ − Vdc) at the dc grid, which is then fed into a proportional integral controller to generate a current reference i∗ d for id to track. To eliminate the presence of high frequency switching ripples at the dc grid, Vdc is first passed through a first-order LPF. The current i q is controlled to be zero so that the PMSG only delivers real power. The current errors Δid and Δiq are then converted into the abc frame and fed into a proportional resonant (PR) controller to generate the required control signals using pulse-width modulation.

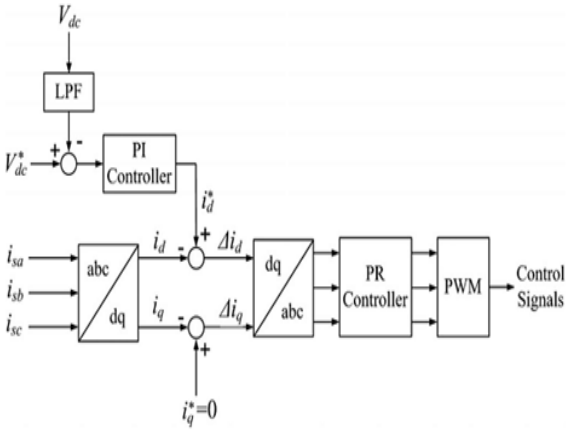

Fig. 4. Configuration of the proposed controller for the ac/dc converter.

Control Design for the DC/AC Inverter

In order for the microgrid to operate in both grid-connected and islanded modes of operation, a model-based controller using MPC is proposed for the control of the inverters. MPC is a model-based controller and adopts a receding horizon approach in which the optimization algorithm will compute a sequence of control actions to minimize the selected objectives for the whole control horizon, but only execute the first control action for the inverter. At the next time step, the optimization process is repeated based on new measurements over a shifted prediction horizon. To derive the control algorithm for the inverters, the state-space equations are transformed into augmented state-space equations by defining the incremental variables in the following format:

$$\Delta\xi(k) = \xi(k) - \xi(k-1) \quad (17)$$

where ξ represents each variable in the inverter model, such as vDG,iDG, i and u as shown in Fig. 3. By defining the incremental variables, the augmented statespace model for the inverter model operating in the CCM during grid-connected operation can be expressed as follows:

$$x_g(k+1) = A_{g\_aug}X_g(k) + B_{g1\_aug}V_g(k) + B_{g2\_aug}U_g(k) \quad (18)$$

$$Y_g(k) = C_{g_{aug}}X_g(k) \quad (19)$$

Similarly, the augmented state-space model for the inverter model operating in the VCM during islanded operation can be expressed as follows:

$$X_i(k+1) = A_{i\_aug}X_i(k) + B_{i\_aug}U_i(k) \quad (20)$$

$$Y_i(k) = C_{i_{\_aug}}X_i(k) \quad (21)$$

Where

Xi(k) = [Δi(k) ΔvDG(k) ΔiDG(k) vDG(k)]^T is the state vector; Ui(k) = Δui(k) is the control signal; and Yi(k) = vDG(k) is the output. For the control of the two augmented models in the CCM and the VCM, the following cost function is solved using quadratic programming in the proposed MPC algorithm.

$$J = (R_s - Y_j)^T + U_j{}^T Q U_j \quad (22)$$

After the control signal u is generated by the MPC algorithm, it will be applied to the dc/ac inverter as shown in Fig. 3.

NUMERICAL SIMULATION ANALYSIS

The simulation model of the proposed dc grid based wind power generation system shown in Fig. 1 is implemented in MATLAB/Simulink. The effectiveness of the proposed design concept is evaluated under different operating conditions when the microgrid is operating in the grid-connected or islanded mode of operation. The system parameters are given in Table I. The impedances of the distribution line are obtained from. In practical implementations, the values of the converter and inverter loss resistance are not precisely known. Therefore, these values have been coarsely estimated.

TABLE I
PARAMETERS OF THE PROPOSED SYSTEM

Parameter	value
Distribution grid voltage	$v_g = 230V\ (Phase)$
Dc grid voltage	$V_{dc} = 500V$
PMSG stator impedance	$R_s = 0.2\Omega, L_s = 2.4mH$
Distribution line impedance	$R_l = 7.5m\Omega, L_l = 25.7\mu H$
Inverter LC filter	$L_f = 1.2mH, C_f = 20\mu F$
Converter capacitor	C=300 μF
Converter and inverter loss resistance	R=1mΩ
Load 1 rating	$P_{L1} = 35kW, Q_{L1} = 8kVAr$
Load 2 rating	$P_{L2} = 25kW, Q_{L2} = 4kVAr$

Test Case 1: Failure of One Inverter During Grid-Connected Operation

When one of the inverters fails to operate and needs to be disconnected from the dc grid, the other inverter is required to handle all the power generated by the PMSGs. In this test case, an analysis on the microgrid operation when one of the inverters is disconnected from operation is conducted.

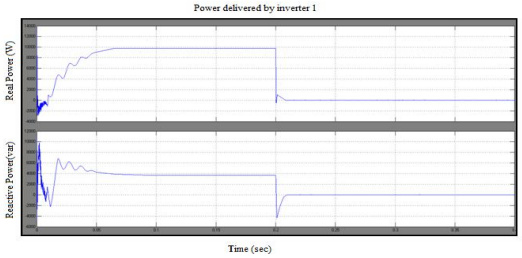

Fig. 5. Real (top) and reactive (bottom) power delivered by inverter 1.

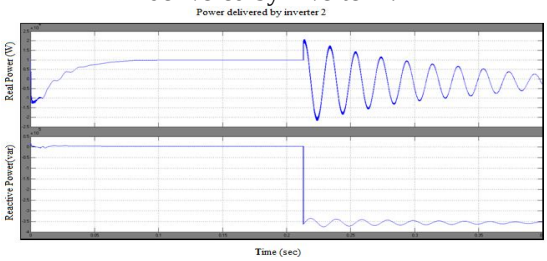

Fig. 6. Real (top) and reactive (bottom) power delivered by inverter 2

Figs. 5 and 6 show the waveforms of the real and reactive power delivered by inverters 1 and 2 for $0 \leq t < 0.4$ s respectively. For $0 \leq t < 0.2$ s, both inverters 1 and 2 are in operation and each inverter delivers about 10 kW of real power and 4 kVAr of reactive power to the loads.

The remaining real and reactive power that is demanded by the loads is supplied by the grid which is shown in Fig. 7. It can be seen from Fig. 7 that the grid delivers 40 kW of real power and 4 kVAr of reactive power to the loads for $0 \leq t < 0.2$ s.

Fig. 7. Real (top) and reactive (bottom) power delivered by the grid.

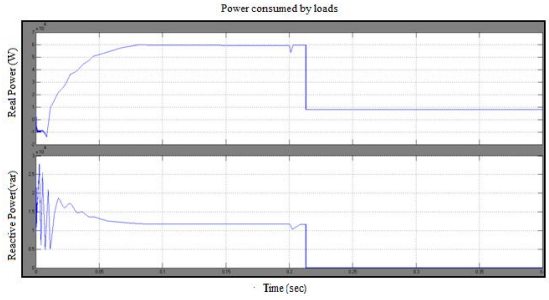

Fig. 8. Real (top) and reactive (bottom) power consumed by the loads.

This undelivered power causes a sudden power surge in the dc grid which corresponds to a voltage rise at t = 0.2 s as shown in Fig. 9.

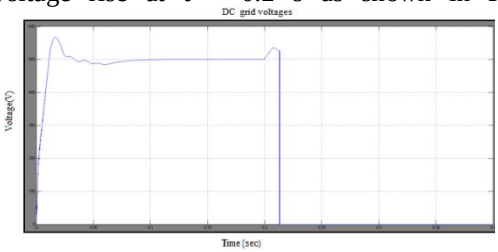

Fig. 9. DC grid voltage.

It is observed from Fig. 9 that the voltage at the dc grid corresponds to a voltage dip at t = 0.26 s due to the increase in power drawn by inverter 2 and then returns to its nominal value of 500 V for $0.26 \leq t < 0.4$ s. As observed in Fig. 8, at t = 0.26 s, the changes in power delivered by inverter 2 and the grid also cause a transient in the load power.

Test Case 2: Connection of AC/DC Converter During Grid-Connected Operation

The real power generated from each of the remaining three PMSGs is maintained at 5.5 kW and their aggregated real power of 16.5 kW at the dc grid is converted by inverters 1 and 2 into 14 kW of real power and 8 kVAr of reactive power. As shown in Figs. 10 and 11, each inverter delivers real and reactive power of 7 kW and 4 kVAr to the loads respectively. The rest of the real and reactive power demand of the loads is supplied by the grid as shown in Fig. 12.

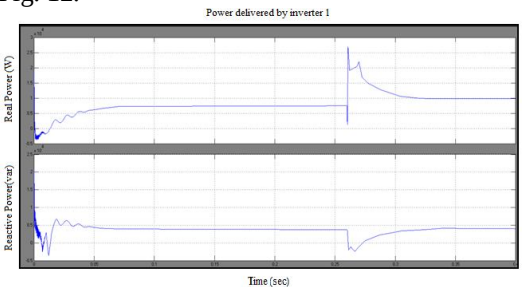

Fig. 10. Real (top) and reactive (bottom) power delivered by inverter 1.

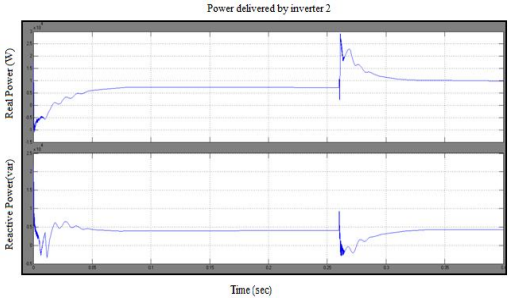

Fig. 11. Real (top) and reactive (bottom) power delivered by inverter 2

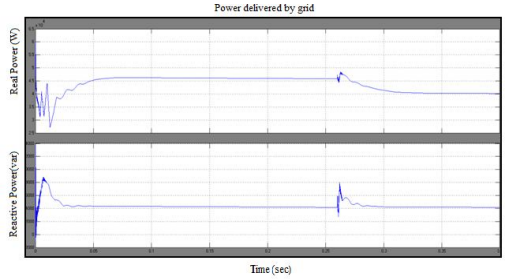

Fig. 12. Real (top) and reactive (bottom) power delivered by the grid.

It can be seen from Fig. 12 that the grid delivers 46 kW of real power and 4 kVAr of reactive power to the loads. At t = 0.2 s, PMSG A which generates real power of 5.5 kW is connected to the dc grid. This causes a sudden power surge at the dc grid and results in a voltage rise at t = 0.2 s as shown in the voltage waveform of Fig. 13. At t = 0.26 s, the EMS increases the real delivered by each inverter to 10 kW while the reactive power supplied by each inverter remains unchanged at 4 kVAr as shown in Figs. 10 and 11.

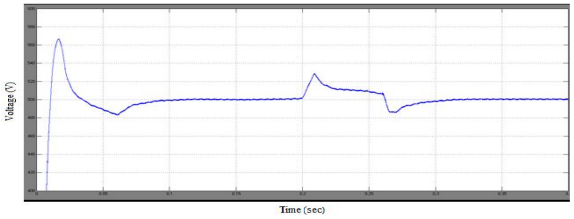

Fig. 13. DC grid voltage.

The grid also simultaneously decreases its supply to 40 kW of real power for $0.26 \leq t < 0.4$ s while its reactive power remains constant at 4 kVAr as shown in Fig. 12.

Test Case 3: Islanded Operation When the microgrid operates islanded from the distribution grid, the total generation from the PMSGs will be insufficient to supply for all the load demand.

Fig. 14. Real (top) and reactive (bottom) power delivered by the grid.

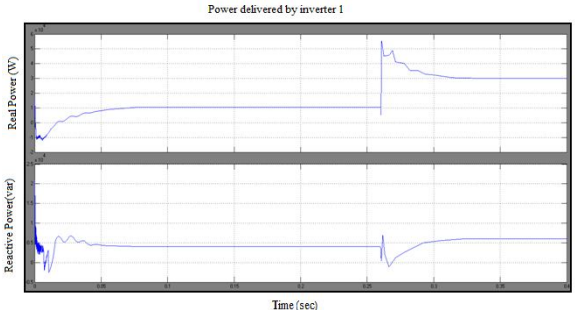

Fig. 15. Real (top) and reactive (bottom) power delivered by inverter 1.

The microgrid is initially operating in the grid-connected mode. The grid is supplying real power of 40 kW and reactive power of 4 kVAr to the loads for $0 \leq t < 0.2$ s as shown in Fig. 14 while each inverter is delivering real power of 10 kW and reactive power of 4 kVAr to the loads as shown in Figs. 15 and 16. At t = 0.2 s, the microgrid is disconnected from the distribution grid by the CBs due to a fault occurring in the upstream network of the distribution grid.

Fig. 16. Real (top) and reactive (bottom) power delivered by inverter 2.

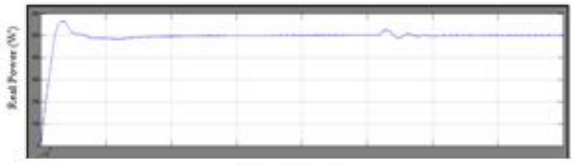

Fig. 17. Real power delivered by SB.

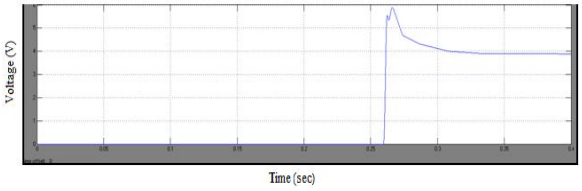

Fig. 18. DC grid voltage.

At the same time, the real and reactive power delivered by each inverter is also increased by the EMS to 30 kW and 6 kVAr as shown in Figs. 15 and 16 respectively. Fig. 18 shows the dc grid voltage

where slight voltage fluctuations are observed at t = 0.26 s.

CONCLUSION

The design of dc grid based wind power generation system in a microgrid , is proposed in this paper that enables parallel operation of several WGS in a poultry farm. As we compare to traditional wind power generation systems, the proposed system design mitigates the need for voltage and frequency synchronization, it will allows the WGs to be switched on or off with minimal disturbances to the microgrid operation. The design and performance of microgrid system is analyze through MATLAB simulation. Moreever the proposed control system configuration still requires assist reenactment approval since measurement errors because of errors of the voltage and current sensors, and displaying errors because of varieties in actual errors parameters, for example, distribution line and transformer impedances will influence the performance of the controller in practical implementation . In addition, MPC depends on the exactness of model foundation, henceforth additionally explore on enhancing the controller vigor to demonstrating inaccuracy is required. The simulation results about got and the examination performed in this paper serve in as a reason for the design of a dc system based wind power control generation system in a microgrid.

REFERENCES

[1] M. Czarick and J. Worley, “Wind turbines and tunnel fans,” Poultry Housing Tips, vol. 22, no. 7, pp. 1–2, Jun. 2010.

[2] The poultry guide: Environmentally control poultry farm ventilation systems for broiler, layer, breeders and top suppliers. [Online]. Available: http://thepoultryguide.com/poultry-ventilation/

[3] Livestock and climate change. [Online]. Available: http://www. worldwatch.org/files/pdf/Livestock%20and%20Climate%20Change.pdf.

[4] Farm Energy: Energy efficient fans for poultry production. [Online]. Available: http://farmenergy.exnet.iastate.edu.

[5] A. Mogstad, M. Molinas, P. Olsen, and R. Nilsen, “A power conversion system for offshore wind parks,” in Proc. 34th IEEE Ind. Electron., 2008, pp. 2106–2112

. [6] A. Mogstad and M. Molinas, “Power collection and integration on the electric grid from offshore wind parks,” in Proc. Nordic Workshop Power Ind. Electron., 2008, pp. 1–8. [7] D. Jovic, “Offshore wind farm with a series multiterminal CSI HVDC,” Elect. Power Syst. Res., vol. 78, no. 4, pp. 747–755, Apr. 2008.

[8] X. Lu, J. M. Guerrero, K. Sun, and J. C Vasquez “An improved droop control method for DC microgrids based on low bandwidth communication with DC bus voltage restoration and enhanced current sharing accuracy,” IEEE Trans. Power Electron., vol. 29, no. 4, pp. 1800–1812, Apr. 2014.

[9] T. Dragicevi, J. M. Guerrero, and J. C Vasquez, “A distributed control strategy for coordination of an autonomous LVDC microgrid based on power-line signaling,” IEEE Trans. Ind. Electron., vol. 61, no. 7, pp. 3313–3326, Jul. 2014.

[10] N. L. Diaz, T. Dragicevi, J. C. Vasquez, and J. M. Guerrero, “Intelligent distributed generation and storage units for DC microgrids—A new concept on cooperative control without communications beyond droop control,” IEEE Trans. Smart Grid, vol. 5, no. 5, pp. 2476–2485, Sep. 2014.